Self-Biased Magnetoelectric Ni/LiNbO₃/Ni Trilayers for Body-Embedded Electronic Energy Harvesters

Tianwen Huang,[1,2,*] Loïc Becerra,[3] Aurélie Gensbittel®,[1,2] Yunlin Zheng,[3] Hakeim Talleb,[1,2]
Ulises Acevedo Salas,[1,2] Zhuoxiang Ren,[1,2] and Massimiliano Marangolo®[3]

[1]*Sorbonne Université, CNRS, Laboratoire de Génie Electrique et Electronique de Paris, Paris 75252, France*

[2]*Laboratoire de Génie Electrique et Electronique de Paris, Université Paris-Saclay, CentraleSupélec, CNRS, Gif-sur-Yvette 91192, France*

[3]*Sorbonne Université, CNRS, Institut des NanoSciences de Paris, INSP, UMR7588, Paris 75005, France*

In this study, we present the fabrication and characterization of Ni/LiNbO₃/Ni trilayers using rf sputtering. These trilayers exhibit thick Ni layers (10 µm) and excellent adherence to the substrate, enabling high magnetoelectric coefficients. By engineering the magnetic anisotropy of nickel through anisotropic thermal residual stress induced during fabrication, and by selecting a carefully chosen cut angle for the LiNbO₃ substrate, we achieved self-biased behavior. We demonstrate that these trilayers can power medical implant devices remotely using excitation by a small ac magnetic field, thereby eliminating the need for a dc magnetic field and bulky magnetic field sources. The results highlight the potential of these trilayers for the wireless and noninvasive powering of medical implants. This work contributes to the advancement of magnetoelectric materials and their applications in healthcare technology.

I. INTRODUCTION

Research efforts on magnetoelectric (ME) composites open perspectives in different engineering domains for designing sensors, transducers, filters, and other devices based on the change of P (electric polarization) by an excitation magnetic field (direct ME effect) or by the change of M (magnetization) through an excitation electric field (converse ME effect). Particularly exciting is the possibility to direct electric power obtained by ME energy harvesters from a magnetic field excitation source to embedded medical components [1]. In this biomedical context, recent articles have shown the feasibility that an embedded sensor chip can be powered by a neighboring ME resonator activated, through the human body, by a weak dynamic magnetic field working in a frequency range that is transparent through the human body (hundreds of kHz) while respecting the exposure limit value (1 Oe) [2–5].

Among the most promising ME devices, there are 2–2-type laminate composites constituted of ferroelectric (FE) compounds (e.g., BaTiO₃, Pb(Zr, Ti)O₃, Pb(Mg, Nb)O₃-PbTiO₃) intimately connected to ferromagnetic (FM) and giant magnetostrictive materials (e.g., CoFe₂O₄, Terfenol-D, Galfenol), leading to efficient cross coupling via intense mechanical elastic strain [6]. The efficiency is measured by the ME coefficient, α_E, expressed as $dE/dH = V_{ME}/(H_{ac}t_p)$, where t_p is the thickness of the piezoelectric substrate, H_{ac} is an external small dynamic magnetic field (~ 1 Oe) under static magnetic field H_{dc} applied to the magnetostrictive layer, and V_{ME} is the voltage induced across the electrodes of the piezoelectric transducer. It is important to notice that α_E depends on the so-called piezomagnetic coefficient ($q = d\lambda/dH_{ac}$, where λ is the magnetostriction strain), which is usually significant around the static magnetic bias field, H_{bias} ($\sim$ several hundred Oe). Consequently, the ME devices need to be immersed in a static magnetic field generated by bulky permanent magnets or electromagnets and excited by a small dynamic field generated by an external coil or solenoid.

Although, in general terms, the requirements of a ME device depend on its functionality, a set of requirements is crucial for any application:

(i) Reliability versus cycling: fatigue and aging of the adhesive binding are usually observed in (epoxy-)glued laminates undergoing fluctuating stresses and strains. Various epoxy-free methods have been developed in the last two decades to circumvent these limitations [7].

(ii) Rare-earth-free and lead-free structures to minimize environmental and health issues: Lead Zirconium Titanate, with the chemical formula Pb[Zr$_x$Ti$_{1-x}$]O₃ ($0 \leq x \leq 1$) (PZT) and Nd₂Fe₁₄B alloys should be avoided, despite

_____
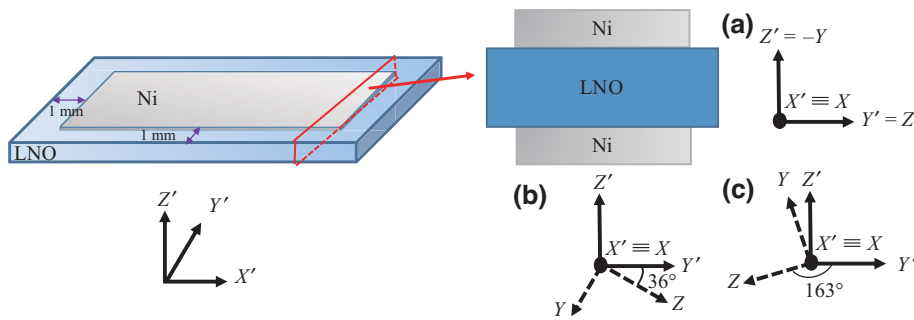*tianwen.huang@sorbonne-universite.fr

FIG. 1. Illustration of different cuts of single-crystal LiNbO$_3$ substrate: (a) Y cut, (b) 36° Y cut, (c) 163° Y cut.

their optimal piezoelectric and magnetostrictive properties [8]. Particular care must be taken for medical applications where materials function *in vivo* without eliciting detrimental responses in the body.

(iii) Low-size and low-cost architectures: integrated permanent magnets to generate bias fields represent a serious bottleneck for the elaboration of compact and cheap devices. Self-biased systems permit the ME effect in the absence of a static magnetic bias field, H_{dc} [9].

Recent articles reported promising results that fulfilled all the aforementioned requirements. Nan *et al.* [8] elaborated compact, power-efficient, and self-biased magnetoelectric nanoelectromechanical system resonators constituted of AlN/(Fe-Ga-B/Al$_2$O$_3$) ×10. Self-biasing is due to magnetic domain-wall motion that is not zero at zero-bias magnetic field and changes the Young's modulus. These sensors were produced by sputtering, which guaranteed reliable adhesion between the layers. Lage *et al.* adopted exchange bias between Mn$_{70}$Ir$_{30}$ and Fe$_{50}$Co$_{50}$ grown on piezoelectric AlN to self-bias ME cantilevers [10]. Built-in stress during heterostructure preparation can induce self-biasing in 2-2 systems, as shown in BaTiO$_3$–

(Ni$_{0.8}$Zn$_{0.2}$)Fe$_2$O$_4$ multilayers [11] and Ni/PZT/Ni multilayers [12], which are grown by cofiring and electrochemical deposition, respectively.

The self-biased ME effect can be obtained by tailoring the ferromagnetic phase or interfacial coupling by varying the FM composition, by designing a functional graded structure, or by imposing a giant built-in stress along the constituent's interface [9]. Nevertheless, growth procedures are not easy to handle and self-biasing is obtained only at very low thickness and consequently low power.

Here, we report a thick ME 2–2-type device composed of two approximately 10-μm-thick layers of magnetostrictive nickel (Ni) and an approximately 100-μm-thick lithium niobate (LiNbO$_3$, LNO) piezoelectric layer. Two different commercially available LiNbO$_3$ cuts were used and compared: 36° Y cut and 163° Y cut. This device is designed to fulfil the aforementioned requirements: reliability versus cycling is assured by the interlayer physical binding obtained by magnetron sputtering growth; self-biasing is ensured in a simple and reproducible way, i.e.,
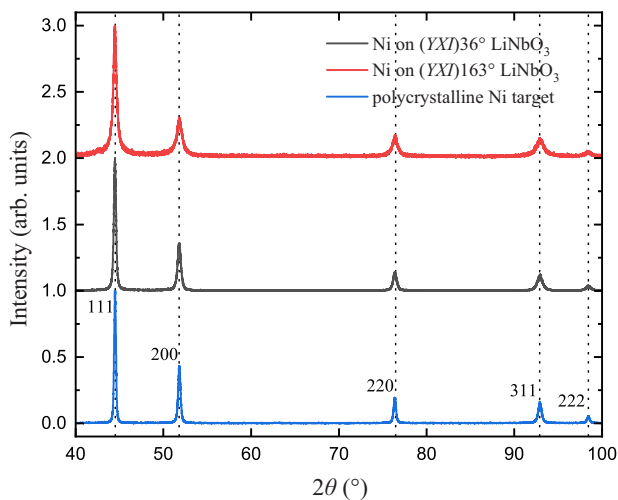

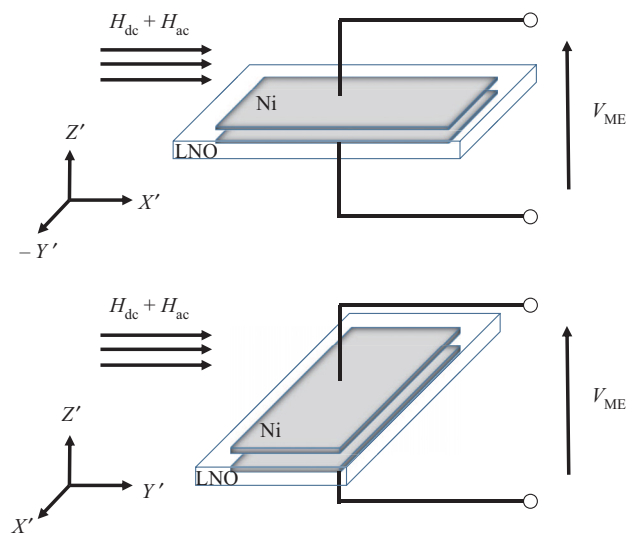FIG. 2. XRD patterns of the deposited Ni films.

FIG. 3. Schematic diagrams of Ni/LiNbO$_3$/Ni trilayer function in *LT* mode.

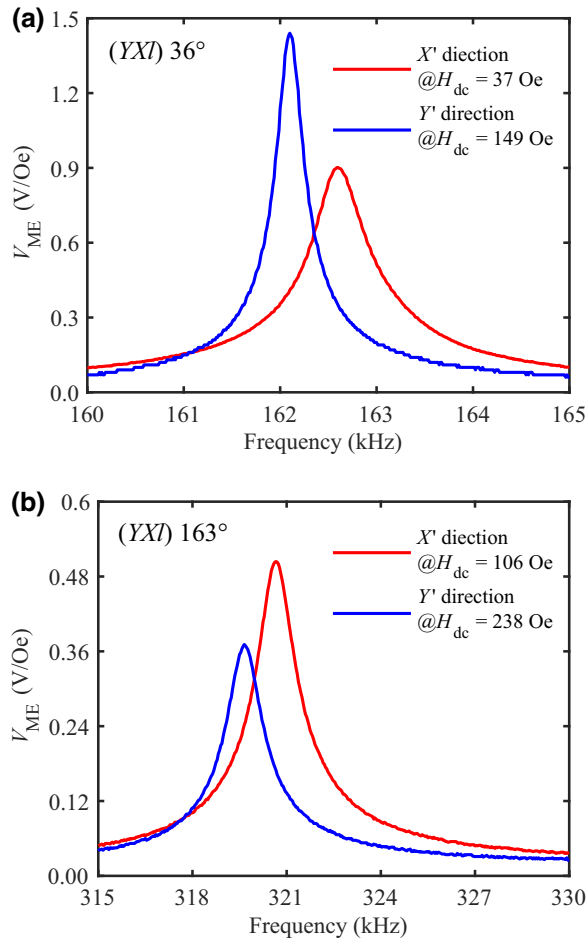FIG. 4. ME resonance measurement as a function of frequency for (a) Ni/$(YXl)36°$ LiNbO$_3$/Ni and (b) Ni/$(YXl)163°$ LiNbO$_3$/Ni samples in X' and Y' directions.

by large in-plane residual stress arising from the thermal-expansion-coefficient mismatch of Ni and LiNbO$_3$.

The dimensions of the samples are designed to obtain the resonant ME effect with work frequencies ranging between 160 and 321 kHz, i.e., in the transparent range through the human body. These properties, combined with the nontoxicity of the two compounds, make the Ni/LiNbO$_3$/Ni system particularly well suited for biomedical-related applications [9]. Admittedly, since nickel allergy is still a potential health problem affecting 10%–20% of the world's population [13,14], encapsulation in a medical catheter can be envisaged.

II. EXPERIMENT

A. Sample preparation

Figure 1 shows the proposed ME laminated samples, in which Ni polycrystalline films (~ 10 μm) are deposited

on a piezoelectric double-side-polished LiNbO$_3$ layer (single crystal) in 36° or 163° Y cuts of $t_p = 100$ μm. Given their ferromagnetic behavior and electrical conduction, the Ni films are deposited on each face by rf sputtering from a high-purity Ni target (Ni > 99.95%) and act both as magnetostrictive layers and as electrodes for LiNbO$_3$.

The crystallographic X-Y-Z axes of the 36° and 163° Y-cut LiNbO$_3$ substrates are identified using in-plane x-ray diffraction (XRD) for detecting the $(2\bar{1}0)$ peak intensity representing the X axis ($\lambda \sim 1.540593$ Å). The observations show that, for each LiNbO$_3$ substrate, the crystallographic X axis is parallel to the X' (length) direction. Thus, according to the IEEE standard [15], we can denote the 36° and 163° Y cuts used more precisely as $(YXl)36°$ and $(YXl)163°$, respectively. Before the sputtering deposition process, each LiNbO$_3$ substrate was chemically prepared with an acetone cleaner in an ultrasonic bath and the surfaces were *in situ* cleaned with argon plasma. The sputtering process on each LiNbO$_3$ substrate face was performed within a chamber under an argon atmosphere at a pressure of 10^{-3} mbar at room temperature and with a supply power of 500 W. In this way, Ni films with a thickness of approximately 10 μm were deposited on both sides of a LiNbO$_3$ substrate without continuous substrate rotation. The growth rate achieved was approximately 55.5 nm/min. Moreover the Ni target and the substrates were in a planar configuration during deposition. As shown in Fig. 1, two gaps of 1 mm between the Ni films and the edges of the LiNbO$_3$ substrate were imposed to avoid potential electrical connection between both Ni films.

Figure 2 shows the XRD patterns of a deposited nickel film compared with the pattern of the reference polycrystalline Ni target. It can be observed that each deposited Ni film on the LiNbO$_3$ substrate behaves similarly to that of the polycrystalline sample. Furthermore, the crystallite sizes of the Ni films on the $(YXl)163°$ LiNbO$_3$ substrate are smaller than those on the $(YXl)36°$ LiNbO$_3$ substrate.

B. Experimental measurements and discussion

1. ME characterization

Figure 3 depicts two magnetic excitation configurations used in LT mode for each ME Ni/LiNbO$_3$/Ni composite. Each composite was excited by an external magnetic field applied longitudinally (L mode) in the X' or Y' in-plane direction, and the electric output voltage was polarized transversely (T mode) in the Z' direction. As previous studies have shown [16,17], the ME coefficient, α_E, is mainly influenced by the transverse piezoelectric coefficient, d_{3i}^P. Consequently, the cuts of $(YXl)36°$ and $(YXl)163°$, presenting high and approximate values, i.e., d_{31}^P and $d_{32}^P = 18$ pC/N, have been selected to favor our study of the ME
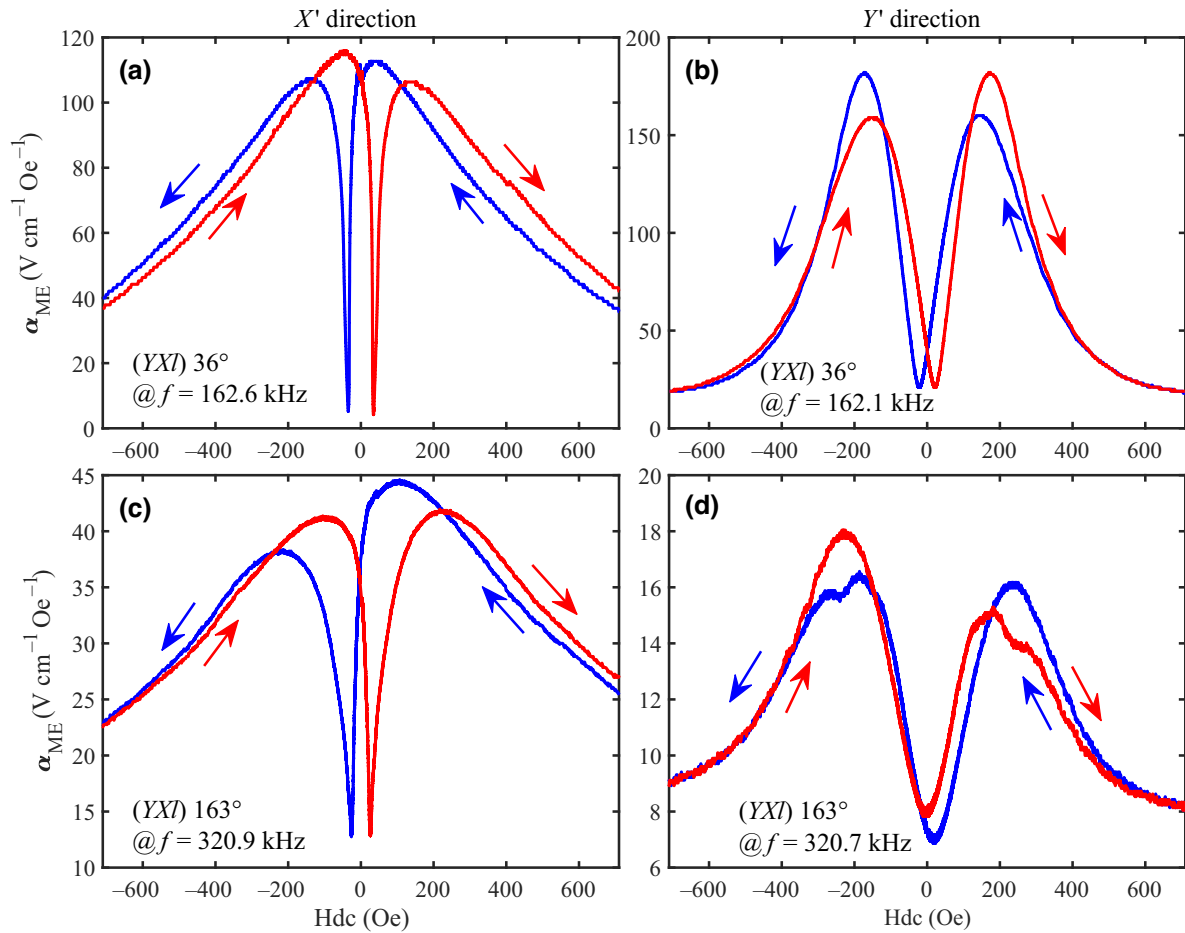
FIG. 5.   ME coefficient as a function of H_{dc} for Ni/$(YXl)36°$ LiNbO$_3$/Ni and Ni/$(YXl)163°$ LiNbO$_3$/Ni samples in X' and Y' directions. Measurements are performed at the ME resonance frequency of each sample.

effect with isotropic piezoelectric effects along the X' and Y' directions, respectively (see Fig. 3).

ME coefficient characterization has been carried out using the experimental setup described in Ref [2]. A copper coil consisting of a hundred turns was used to apply a small harmonic magnetic signal, $H_{ac} = 1$ Oe (in rms). This field was driven by an ac current from an arbitrary waveform generator (Rohde & Schwarz HM8150). Simultaneously, a static magnetic field, H_{dc}, was superimposed in the same direction as the small harmonic magnetic signal, H_{ac}, by adjusting the distance, d, between two opposite permanent magnets mounted on a moving rail. The value of H_{dc} that was related to d was previously calibrated using a gaussmeter with its probe positioned within the center of the copper coil. Each ME sample was then inserted inside the coil to apply the superimposed magnetic field during ME coefficient characterization. A specific support was used for aligning the length or width direction of ME samples with the applied magnetic field. Thus, the ME voltage output (V_{ME}) generated between the Ni layers of

a ME sample was then measured using a digital oscilloscope (Keysight MSO7054A). Finally, the ME coefficient, $\alpha_E = V_{ME}/(H_{ac}t_p)$, could be obtained in a dynamic regime (or a quasistatic regime).

To characterize clearly the ME behavior, α_E versus H_{dc}, of the proposed Ni/LiNbO$_3$/Ni samples, a small harmonic magnetic signal, $H_{ac} = 1$ Oe, was applied around the mechanical resonance (MR) frequency of each sample to obtain maximal mechanical oscillation in an elastic phase. The first longitudinal MR was chosen, and the calculated MR frequencies were 154.2 and 348.1 kHz for the 20-mm- and 10-mm-wide samples, respectively [18]. As shown in Fig. 4, the ME resonance frequency corresponding to the maximum of V_{ME} was identified by ME voltage measurements performed by sweeping the frequency of the H_{ac} signal, and we observed that the measured ME resonance frequencies in two in-plane directions were close to the calculated MR frequencies, as expected. Afterwards, ME coefficient characterization was performed by sweeping H_{dc} first from −710 to 710 Oe and then from 710
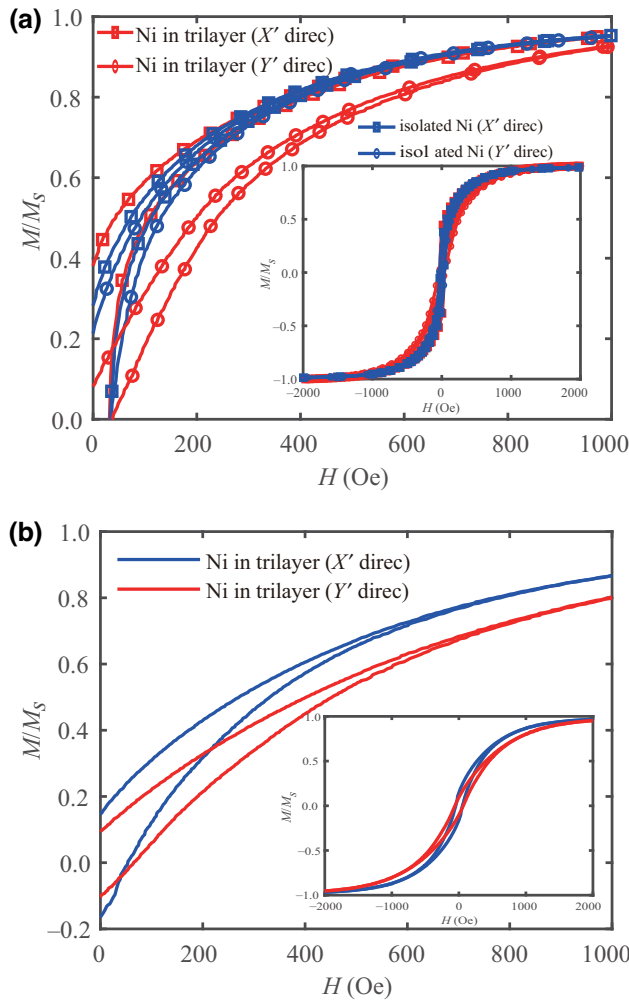
FIG. 6.   (a) Magnetization of nickel films in the Ni/$(YXl)36°$ LiNbO$_3$/Ni trilayer sample and its freestanding state in X' and Y' directions. (b) Magnetization of nickel films in the Ni/$(YXl)163°$ LiNbO$_3$/Ni trilayer sample.

to −710 Oe. We changed the direction of H_{dc} by permuting the permanent magnets in the position of $H_{dc} \approx$ 0 Oe. It is worth noting that this H_{dc} sweep implies the first magnetization of the samples since they have been prepared.

In this study, we investigated the impact of H_{dc} on the resonance frequency of the ME response. Our findings reveal that setting H_{dc} to zero does not result in a significant alteration of the resonance frequency. Furthermore, we observe that the shape of the ME coefficient curve remains unaffected by variations in the excitation frequency, despite the observed decrease in the ME response (see Fig. 4).

As shown in Fig. 5, each measurement has a maximum ME response at the magnetic bias field, H_{bias}. We notice that H_{bias} values in the X' direction are much lower than those in the Y' direction: for Ni/$(YXl)36°$ LiNbO$_3$/Ni, H_{bias}

is equal to ±37 and ±149 Oe in the X' and Y' directions, respectively; for Ni/$(YXl)163°$ LiNbO$_3$/Ni, H_{bias} is equal to ±106 and ±238 Oe in the X' and Y' directions, respectively.

The main findings of our article are shown in Fig. 5, where "self-biased" behavior is reported for the applied magnetic excitation parallel to the X' direction. Interestingly, at $H_{dc} = 0$, α_E is at 94.20% of its maximum value for the sample grown on the Ni/$(YXl)36°$ LiNbO$_3$/Ni substrate and at 80% for the one grown on the Ni/$(YXl)163°$ LiNbO$_3$ substrate. Moreover, the self-biased behavior is lost in the Y' direction, where the α_E values are less than 40% of their maximum values.

Interestingly, by comparing their magnetoelectric responses with the ME trilayer Ni/PZT-5H/Ni composites reported in the literature [19,20], our results showed that our composite materials exhibited a significantly better magnetoelectric response at zero H_{dc}. These findings suggest that the composite material of Ni/LiNbO$_3$/Ni has the potential to be used in the development of advanced magnetoelectric devices.

2. Magnetic anisotropy measurements: Role played by the LiNbO$_3$ substrate

In the following, we relate the ME response of our devices to the intrinsic magnetic properties of Ni films, and we show the important role played by the LiNbO$_3$ substrate. For this purpose, we collected magnetic hysteresis loops by using a vibrating sample magnetometer (VSM). Magnetization (M) was measured at 300 K as a function of H_{dc} from 2 to 500 Oe (step = 10 Oe), then from 500 to −500 Oe with high precision (step = 2 Oe), and from −500 to −2 kOe; finally these steps were repeated in reverse. The samples were laser cut into 5×5 mm^2 pieces to fit in the VSM sample holder. After measuring magnetization of the trilayer sample, we isolated freestanding nickel films, the magnetization of which was measured by using the VSM.

As shown in Fig. 6, anisotropic magnetization behavior is observed for trilayer samples with higher remanence and lower saturation field for the X' direction compared to the Y' direction for the Ni/$(YXl)36°$ LiNbO$_3$/Ni sample. Similar anisotropic magnetization behavior was also observed in the Ni/$(YXl)163°$ LiNbO$_3$/Ni sample. It worth noting that the observed magnetic discrepancy between the two samples can be attributed to the difference in crystallite size, as shown in Fig. 2, affecting the magnetic coupling and alignment of magnetic moments within the films. Interestingly, the anisotropy of the Ni/$(YXl)36°$ LiNbO$_3$/Ni sample is strongly reduced in freestanding films, indicating the important role played by residual stress imposed by the substrate. This allows us to infer that LiNbO$_3$ substrates induce anisotropic internal stress and consequent magnetic anisotropy.
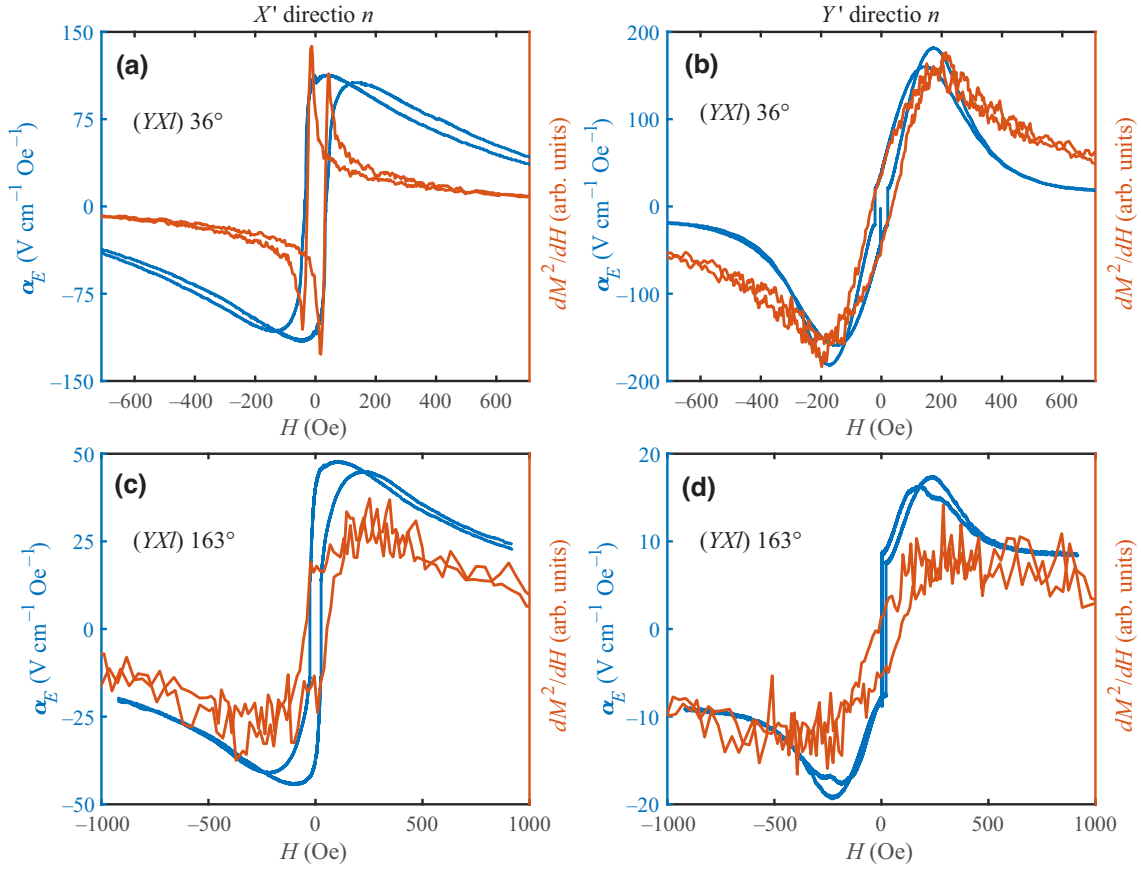
FIG. 7.   ME hysteresis loops and (dM^2/dH)-H curves of trilayer samples in X' and Y' directions.

The magnetocrystalline anisotropic energy is estimated by computing the area between the M-H curves along the X' and Y' directions. This yields 6.72 and 6.87 kJ/m^3 for the Ni/$(YXl)36°$ LiNbO$_3$/Ni and Ni/$(YXl)163°$ LiNbO$_3$/Ni samples, respectively.

3. Relationship between magnetic and ME anisotropy

To relate the magnetic anisotropy to the anisotropic ME response, we compare $M(H)$ cycles with the α_E field dependence. Indeed, ME coupling combines piezomagnetic and piezoelectric effects. Herein, both effects are supposed to be linear. Following Ref. [16], the ME coefficient can be written as the product of the gradients of piezomagnetic and piezoelectric effects:

$$\alpha_E = \left| \frac{\partial T}{\partial S} \times \frac{\partial D}{\partial T} \times \frac{\partial E}{\partial D} \right| \times \frac{\partial S}{\partial H}, \qquad (1)$$

where T is the stress, D is the electric displacement field, E is the electric field, and S is the strain. Thus, the magnetic field dependence of the ME coefficient is such that $\alpha_E \propto \partial S/\partial H = \partial \lambda/\partial H$, where λ is the strain due to magnetostriction. Since $\lambda \propto M^2$, finally, we obtain $\alpha_E \propto$

$\partial M^2/\partial H$ as the relationship connecting the ME response and magnetization.

As shown in Fig. 7, we find a qualitative agreement between the H dependence of $(\partial M^2/\partial H)$ and the ME hysteresis loop (permutating the sign of α_E at the antiresonances), attesting that the ME anisotropy behavior reflects the magnetic anisotropy of nickel films in contact with the LiNbO$_3$ substrates.

4. Origin of magnetic and ME anisotropy

Below, we show that the origin of the magnetic anisotropy resides in the mismatch between the coefficients of thermal expansion (CTEs) of Ni and LiNbO$_3$ as the prevailing view [21–23]. Indeed, the samples are heated up

TABLE I.   CTEs of nickel α_f and LNO substrates α_s.

	α in X' direction (K^{-1})	α in Y' direction (K^{-1})
Nickel	13.4×10^{-6}	13.4×10^{-6}
$(YXl)36°$ LiNbO$_3$	15.4×10^{-6}	10.23×10^{-6}
$(YXl)163°$ LiNbO$_3$	15.4×10^{-6}	8.18×10^{-6}

TABLE II. In-plane strain determined by XRD of the Ni (311) reflection along X' and Y' directions in Ni in the trilayer and in the isolated Ni layer. The standard error of the last significant digit of the values is indicated in parentheses.

	Ni in trilayer (X' direction)	Isolated Ni (X' direction)	Ni in trilayer (Y' direction)	Isolated Ni (Y' direction)
2θ (deg)	93.040(3)	93.013(3)	92.983(3)	93.032(4)
d_{311} (Å)	1.06246(3)	1.06269(3)	1.06296(3)	1.06253(3)
strain (%)		−0.022(5)		0.041(6)

during deposition due to exposure to the plasma and cooled down to ambient temperature ($\approx$ 300 K) after the sputtering growth procedure. Thus, the nickel films in the trilayer samples are prone to residual stresses, σ_r, related to thermal expansion effects, i.e.,

$$\sigma_{r,ii} = C_{e,iikl}(\alpha_s - \alpha_f)_{kl}\Delta T, \qquad (2)$$

where α_s and α_f are, respectively, the coefficients of thermal expansion of the LiNbO$_3$ substrate and Ni film; ΔT is the difference between ambient temperature and the temperature during the sputtering deposition process; and $C_{e,iikl}$ is a longitudinal coefficient in the elastic tensor of the Ni film. In the following, we focus on the in-plane biaxial (residual) stress induced in the Ni films, i.e., $\sigma_{r,xx}$ and $\sigma_{r,yy}$. Since the CTE of the LiNbO$_3$ substrate in the X' direction is greater than the CTE of Ni, as shown in Table I ($\alpha_s - \alpha_f > 0$), negative (compressive) residual stress increases upon cooling the sample. In contrast, the coefficient of thermal expansion of the LiNbO$_3$ substrate in the Y' direction is smaller than the CTE of Ni, as shown in Table I ($\alpha_s - \alpha_f < 0$), leading to a positive (tensile) residual stress under cooling conditions. Thus, the residual stress is anisotropic at room temperature, leading to the observed magnetic anisotropy. Indeed, the order of magnitude of residual stress can be evaluated by considering $\Delta T \sim 100$ K due to the growth procedure and the Young's modulus of nickel, $E = 207$ GPa. It turns out that the expected residual stress, σ_r, will be in the order of 50 MPa, with opposite signs in the X' and Y' directions. Hence, the expected magnetic anisotropy energy resulting from these two in-plane stresses is given by

$$K_{u,\sigma} = 2 \times \frac{3}{2} \times \sigma \times \lambda_S, \qquad (3)$$

with $\lambda_S = -34 \times 10^{-6}$ [23]. Thus, we estimated $K_{u,\sigma} \sim 5.1$ J/m^3, in line with the qualitative magnetic anisotropy energies from Fig. 6.

Indeed, it is well known that such values can induce magnetic anisotropy in much thinner Ni films (35 nm), as demonstrated in Ref. [24], when stress is applied statically by an electrostatic ([Pb(Mg$_{0.33}$Nb$_{0.66}$)O$_3$]$_{0.68}$-[PbTiO$_3$]$_{0.32}$) actuator, and in Ref. [25], where stress is applied by deforming a LiNbO$_3$ substrate.

5. Probing stress-induced magnetic anisotropy by magnetic and structural measurements

In the following, we corroborate our hypothesis of residual thermal-stress-induced magnetic anisotropy through two distinct experiments conducted on our two samples. However, the (311)-crystal-plane intensity measured by the in-plane XRD method in the Ni films of the Ni/(YXl)163° LiNbO$_3$/Ni sample was weak, leading to noisy results. Consequently, we focus our analysis on
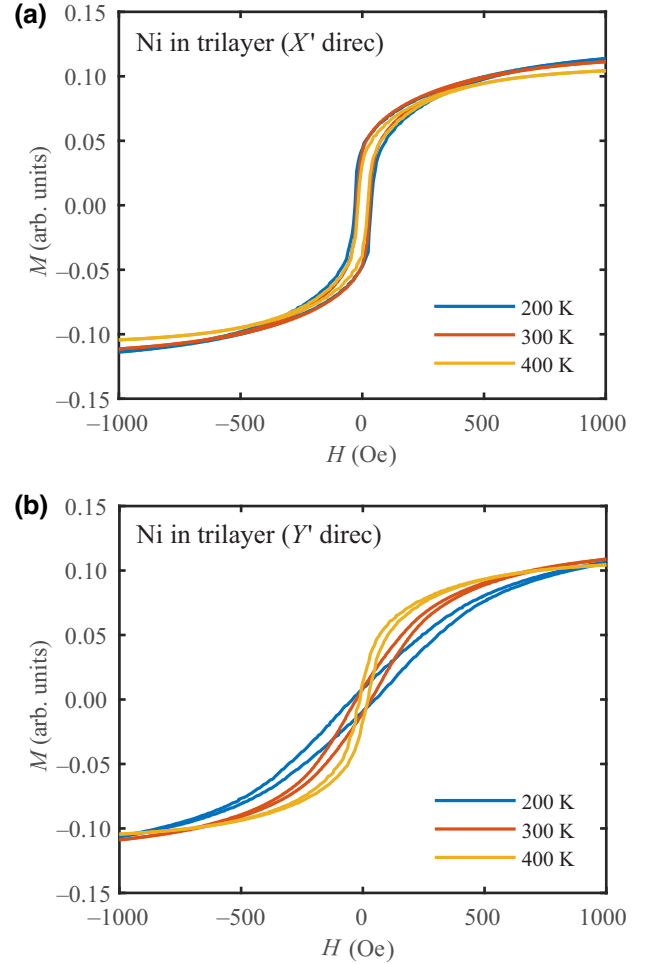
FIG. 8. VSM magnetization cycles were measured at different temperatures in the two in-plane directions of the Ni/(YXl)36° LiNbO$_3$/Ni trilayer: (a) along X' direction. (b) along Y' direction.

the Ni/(*YXl*)36° LiNbO$_3$/Ni sample in the following; this sample provides clearer and more reliable data.

(i) *M*(*H*) curves under different temperatures

In Fig. 8, we report the magnetization cycles measured by using a VSM in the *X'* and *Y'* directions, as a function of temperature. It turns out that the magnetization cycles are strongly temperature dependent along the *Y'* direction: magnetic remanence is higher at 400 K than at 200 K. In the *X'* direction, high remanence is found at all the probed temperatures. This indicates that residual stress is released by heating, leading to more isotropic magnetic behavior at 400 K. This behavior resembles that observed in Fig. 6, where magnetization cycles of freestanding films are strongly modified in the *Y'* direction with respect to clamped trilayers.

(ii) Determination of residual stresses using the x-ray diffraction method

Finally, according to Ref. [21], we confirmed the existence of residual stresses by a direct and quantitative determination of atomic spacing changes to the nickel film by in-plane XRD phi scanning along the *X'* and *Y'* directions. We compared the atomic spacing corresponding to the (311) peak, d_{311}, in the Ni film deposited on the LiNbO$_3$ substrate with the freestanding Ni film after removal from the substrate. As shown in Fig. 9, by fitting of the measured (311) peaks using the pseudo-Voigt function, we could estimate d_{311} in the *X'* and *Y'* directions. As shown in Table II, the measured negative (positive) atomic spacing change signifies the presence of negative (positive) residual stress in the *X'* (*Y'*) direction. Using a Young's modulus of 207 GPa and Poisson's ratio of 0.29 for the Ni material, a temperature change, ΔT, of approximately −70 K can be derived. However, the temperature change
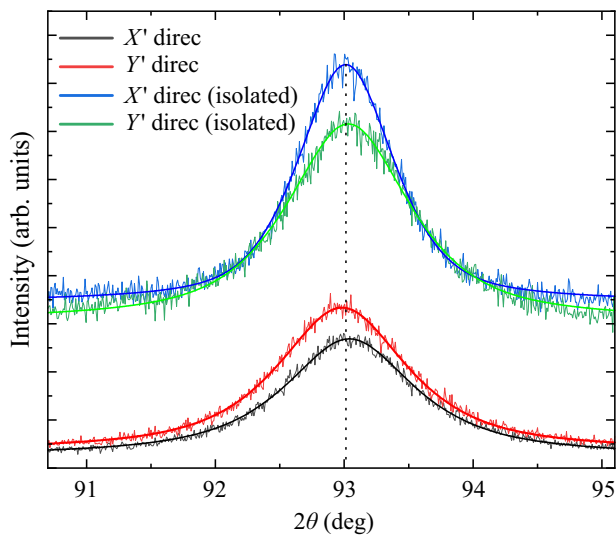
of −70 K involved is slightly lower than the estimated temperature change of −100 K from deposition. The difference can be attributed to the fact that grazing-incidence in-plane XRD measurements primarily capture the top part of the Ni films, rather than the portion in contact with the LiNbO$_3$ substrate.

III. CONCLUSION

In this work, we have shown that Ni/LiNbO$_3$/Ni trilayers allow us to envisage efficient self-biased magnetoelectric devices. The growth of these lead-free and rare-earth-free trilayers by magnetron sputtering guarantees tight and resistant physical binding between the magnetostrictive and piezoelectric layers, with respect to epoxy-assisted adhesive binding, which is prone to fatigue and aging. Ni layers are thick (10 µm each), inducing significant longitudinal deformations of the LiNbO$_3$ layer ($\sim$ 100 µm) and consequent high-ME output ($\sim$ 100 V/cm Oe) in the approximately 100–300 kHz regime. Through the judicious choice of the crystalline orientation of the LiNbO$_3$ substrate (i.e., 36° *Y* cut and 163° *Y* cut), anisotropic residual stress is induced spontaneously in the Ni layers during cooling after growth, as attested to by x-ray diffraction and magnetometry measurements. We demonstrate that residual stresses are due to the thermal-expansion-coefficient mismatch of Ni and LiNbO$_3$, which, in turn, induces significant magnetic anisotropy and consequent self-biasing of the device.

Thus, Ni/LiNbO$_3$/Ni has the potential to enhance its self-biased properties by controlling the residual stress thermally. These findings suggest that the Ni/LiNbO$_3$/Ni composite may have potential applications in the development of self-biased magnetoelectric devices, and we observe that the ME-coefficient responses of Ni/LiNbO$_3$/Ni are better than that of Ni/PZT-5H/Ni reported in the literature.

This study opens the way to a transformative leap forward in magnetoelectric technology for implanted medical devices. Indeed, self-biased Ni/LiNbO$_3$/Ni trilayer composites grown by using physical tools could be the building block for a biocompatible, corrosion-resistant, and durable device based on cycling power supplies that could be charged by an external tiny ($\sim$ 1 Oe) oscillating magnetic field without the need for any dc field, avoiding bulky and expensive magnetic field sources.

FIG. 9.   In-plane XRD patterns of the (311) peak of Ni from the sample comprised of (*YXl*)36° LiNbO$_3$.

———————

[1] M. Paluszek, D. Avirovik, Y. Zhou, S. Kundu, A. Chopra, R. Montague, and S. Priya, Magnetoelectric composites for medical application, Composite Magnetoelectrics; Srinivasan, G., Priya, S., Sun, NX, Eds , 297 (2015).

[2] K. Malleron, A. Gensbittel, H. Talleb, and Z. Ren, Experimental study of magnetoelectric transducers for power supply of small biomedical devices, Microelectronics J. **88,** 184 (2019).

[3] T. Rupp, B. D. Truong, S. Williams, and S. Roundy, Magnetoelectric transducer designs for use as wireless power receivers in wearable and implantable applications, Materials **12,** 512 (2019).

[4] M. Zaeimbashi, M. Nasrollahpour, A. Khalifa, A. Romano, X. Liang, H. Chen, N. Sun, A. Matyushov, H. Lin, C. Dong *et al.*, Ultra-compact dual-band smart NEMS magnetoelectric antennas for simultaneous wireless energy harvesting and magnetic field sensing, Nat. Commun. **12,** 3141 (2021).

[5] J. C. Chen, P. Kan, Z. Yu, F. Alrashdan, R. Garcia, A. Singer, C. E. Lai, B. Avants, S. Crosby, Z. Li *et al.*, A wireless millimetric magnetoelectric implant for the endovascular stimulation of peripheral nerves, Nat. Biomed. Eng. **6,** 706 (2022).

[6] X. Liang, H. Chen, and N. X. Sun, Magnetoelectric materials and devices, APL Mater. **9,** 041114 (2021).

[7] A. Kumar and A. Arockiarajan, Epoxy-free fabrication techniques for layered/2-2 magnetoelectric composite: A review, Smart Materials and Structures (2022).

[8] C.-W. Nan, M. Bichurin, S. Dong, D. Viehland, and G. Srinivasan, Multiferroic magnetoelectric composites: Historical perspective, status, and future directions, J. Appl. Phys. **103,** 1 (2008).

[9] Y. Zhou, D. Maurya, Y. Yan, G. Srinivasan, E. Quandt, and S. Priya, Self-biased magnetoelectric composites: An overview and future perspectives, Energy Harvesting Syst. **3,** 1 (2016).

[10] E. Lage, C. Kirchhof, V. Hrkac, L. Kienle, R. Jahns, R. Knöchel, E. Quandt, and D. Meyners, Exchange biasing of magnetoelectric composites, Nat. Mater. **11,** 523 (2012).

[11] R. A. Islam and S. Priya, Magnetoelectric properties of the lead-free cofired BaTiO₃–(ni₀.₈Zn₀.₂)Fe₂O₄ bilayer composite, Appl. Phys. Lett. **89,** 152911 (2006).

[12] N. Poddubnaya, D. Filippov, V. Laletin, A. Aplevich, and K. Yanushkevich, Magnetoelectric properties of Ni-PZT-Ni heterostructures obtained by electrochemical deposition of nickel in an external magnetic field, Magnetochemistry **9,** 94 (2023).

[13] J. P. Thyssen and T. Menné, Metal allergy–a review on exposures, penetration, genetics, prevalence, and clinical implications, Chem. Res. Toxicol. **23,** 309 (2010).

[14] S. E. Jacob, J. N. Moennich, B. A. McKean, M. J. Zirwas, and J. S. Taylor, Nickel allergy in the united states: A public health issue in need of a "nickel directive", J. Am. Acad. Dermatol. **60,** 1067 (2009).

[15] I. S., Coordinating Committee 11, *Logic Symbols and Diagrams: IEEE Standard Graphic Symbols for Logic Functions; IEEE Standard for Logic Circuit Diagrams* (IEEE, 1987).

[16] Y. Zhou, S. Chul Yang, D. J. Apo, D. Maurya, and S. Priya, Tunable self-biased magnetoelectric response in homogenous laminates, Appl. Phys. Lett. **101,** 232905 (2012).

[17] F. Yang, Y. Wen, P. Li, M. Zheng, and L. Bian, Resonant magnetoelectric response of magnetostrictive/piezoelectric laminate composite in consideration of losses, Sens. Actuators A: Phys. **141,** 129 (2008).

[18] J. Wan, Z. Li, Y. Wang, M. Zeng, G. Wang, and J.-M. Liu, Strong flexural resonant magnetoelectric effect in Terfenol-D/epoxy-Pb(Zr, Ti)O₃ bilayer, Appl. Phys. Lett. **86,** 202504 (2005).

[19] K. Bi, Y. Wang, and W. Wu, Tunable resonance frequency of magnetoelectric layered composites, Sens. Actuators A: Phys. **166,** 48 (2011).

[20] D. Pan, J. Tian, S. Zhang, J. Sun, A. Volinsky, and L. Qiao, Geometry effects on magnetoelectric performance of layered Ni/PZT composites, Mater. Sci. Eng.: B **163,** 114 (2009).

[21] M. Huff, Residual stresses in deposited thin-film material layers for micro- and nano-systems manufacturing, Micromachines **13,** 2084 (2022).

[22] T.-A. Truong, T.-K. Nguyen, H. Zhao, N.-K. Nguyen, T. Dinh, Y. Park, T. Nguyen, Y. Yamauchi, N.-T. Nguyen, and H.-P. Phan, Engineering stress in thin films: An innovative pathway toward 3D micro and nanosystems, Small **18,** 2105748 (2022).

[23] S. A. Mathews and J. Prestigiacomo, Controlling magnetic anisotropy in nickel films on LiNbO₃, J. Magn. Magn. Mater. **566,** 170314 (2023).

[24] S. Finizio, M. Foerster, M. Buzzi, B. Krüger, M. Jourdan, C. A. Vaz, J. Hockel, T. Miyawaki, A. Tkach, S. Valencia *et al.*, Magnetic anisotropy engineering in thin film Ni nanostructures by magnetoelastic coupling, Phys. Rev. Appl. **1,** 021001 (2014).

[25] T. Wu, A. Bur, J. L. Hockel, K. Wong, T.-K. Chung, and G. P. Carman, Electrical and mechanical manipulation of ferromagnetic properties in polycrystalline nickel thin film, IEEE Magn. Lett. **2,** 6000104 (2011).